

Quasi-planar ICME sheath: a cause of first two-step extreme geomagnetic storm of 25th solar cycle observed on 23 April 2023.

Kalpesh Ghag,¹ Anil Raghav^{1*}, Ankush Bhaskar², Shirsh Lata Soni³
Bhagyashri Sathe¹, Zubair Shaikh⁴, Omkar Dhamane¹, Prathmesh Tari¹.

¹Department of Physics, University of Mumbai, Vidyanagari, Santacruz (E), Mumbai 400098, India
²Space Physics Laboratory, Vikram Sarabhai Space Centre, ISRO, Thiruvananthapuram 695022, Kerala,

India

³University of Michigan, 500 S State St, Ann Arbor, MI 48109, USA

⁴Space Sciences Laboratory, University of California, Berkeley, CA 94720, USA

arXiv:2305.05381v2 [physics.space-ph] 12 Jan 2024

*anil.raghav@physics.mu.ac.in

Abstract

Interplanetary Coronal Mass Ejections (ICMEs) are prominent drivers of space weather disturbances and mainly lead to intense or extreme geomagnetic storms. The reported studies suggested that the planar ICME sheath and planar magnetic clouds (MCs) cause extreme storms. Here, we investigated the first two-step extreme geomagnetic storm ($Sym-H \sim -231$ nT) of 25th solar cycle. Our analysis demonstrates the transformation of ICME sheath into quasi-planar magnetic structures (PMS). The study corroborates our earlier reported finding that the less adiabatic expansion in possible quasi-PMS transformed ICME enhanced the strength of the southward magnetic field component. It contributes to the efficient transfer of plasma and energy in the Earth's magnetosphere to cause the observed extreme storm. We found that the magnetosphere stand-off distance reduced to $< 6.6R_E$, and it impacts geosynchronous satellites moving close to $6R_E$.

Introduction

The geomagnetic field has protected life on Earth from its beginning. The magnetosphere shields us from high-energy cosmic ray radiation, solar energetic particles and the steady stream of solar wind-charged particles that emerge from the Sun. Moreover, the Earth's magnetosphere is disturbed due to significant transient events and fast solar wind from the Sun. The geomagnetic field's horizontal component decreases for a few hours during this disturbance, followed by a subsequent recovery; this phenomenon is known as a geomagnetic storm (W. Gonzalez & Mozer, 1974a; W. Gonzalez et al., 1994; Chapman & Bartels, 1940; Kamide, Yokoyama, et al., 1998).

Generally, two current systems developed in the magnetosphere play a major role in geomagnetic storm phenomena, i.e., the Chapman Ferraro current (Chapman & Ferraro, 1931; Chapman & VCA, 1931) and ring current (Dungey, 1961; Akasofu et al., 1963). The geomagnetic storm has three distinct phases: sudden storm commencement (SSC) followed by the initial phase, the main phase, and the recovery phase (Akasofu et al., 1963; Kamide et al., 1997). SSC results from the magnetosphere's sudden compression due to the solar wind's high dynamic pressure. It causes a rapid increase in Chapman Ferraro current, increasing the horizontal components of the Earth's magnetic field (Dessler et al., 1960). Kindly note that the SSC is associated with the onset of geomagnetic storms, but all storms do not show SSC signatures. If the downstream of the interplanetary shock has high density, high pressure, and high solar wind speed, then the horizontal component of the Earth's magnetic field remains high ($\sim 50nT$) for a few hours. Such an enhanced geomagnetic field followed by SSC is referred to as the initial phase of the storm. Following the initial phase, a decrease in the Earth's horizontal magnetic component is observed, termed the storm's main phase. The main phase is related to the southward IMF components of the solar wind. During the main phase, a tremendous amount of energy and particle injection occurs in the magnetosphere. The cause of the main phase is the intensification of the ring current; the higher the ring current magnitude, the stronger the storm (Frank, 1967; Smith & Hoffman, 1973). The duration of the main phase last for about 12 to 24 hours.

It is followed by a storm's recovery phase, in which the Earth's magnetic field recovers to its original ambient value. Generally, the recovery phase of the storm occurs when the southward IMF turns in the northward direction. The ring current's decay or weakening causes the storm's recovery phase. The rate of ring current decay decides the rate of the recovery phase of the storm. Depending on the causing agent of the storm, the time duration of the recovery phase ranges from one day to several days. The decay of the ring current caused by the charge exchange, or by Coulomb interaction, or wave-particle interaction processes (Daglis et al., 1999; Kozyra & Liemohn, 2003; Chen et al., 1997; Jordanova, 2020; Choraghe et al., 2021; A. N. Raghav et al., 2019).

Geomagnetic storms occur when the interplanetary magnetic field (IMF) orients southward and remains southern for a long time ($> 3Hr$) (W. Gonzalez et al., 1994). The re-

connection between the magnetic field lines of the magnetosphere and interplanetary space is controlled by the IMF's south component (B_z) (Fairfield & Cahill Jr, 1966; Dungey, 1961; W. Gonzalez et al., 1994; O'Brien & McPherron, 2000). The long duration southward component of IMF generally observed in *in-situ* observation of 1) Interplanetary Coronal Mass Ejections (ICMEs) (Kamide, Baumjohann, et al., 1998; I. G. Richardson & Cane, 2012; Akasofu, 2018; Echer et al., 2008). 2) Co-rotating Interaction Structures (CIRs) (I. Richardson et al., 2006; B. T. Tsurutani et al., 2006) 3) High Speed Stream (HSS) (Sheeley et al., 1976; Krieger et al., 1973). Especially, ICMEs are responsible significant enhancement of ring currents that results in extreme geomagnetic storms. It is important to note that ICME possesses three distinct structures i.e. forward propagating shock, the orderly magnetised flux rope, and the turbulent region between shock and flux rope called as sheath (Burlaga, 1988; Bothmer & Schwenn, 1997; Kilpua et al., 2012; Zurbuchen & Richardson, 2006). Storms driven by sheath regions have stronger auroral activity, stronger magneto-tail field stretching, larger inner magnetosphere field asymmetry, and larger asymmetric ring currents. In contrast, MC-driven storms have significant ring-current enhancement, much slower increases in auroral activity, more symmetric ring current, and less intense field stretching and convection (Koskinen & Huttunen, 2006; Schwenn et al., 2005; Huttunen et al., 2006; B. Tsurutani et al., 2011).

Space weather is severely affected by such extreme geomagnetic activity. The extreme geomagnetic storm may weaken the geomagnetic field, allowing the energetic particle to penetrate inside the magnetosphere. Many different technologies used in modern life are prone to the extremes of space weather. For instance, during intense auroral events, powerful induced electrical currents are propelled down the surface of the Earth, disrupting electrical power grids and causing oil and gas pipelines to corrode (Boteler, 2003; Marusek, 2007; Boerner et al., 1983). GPS navigation and high-frequency radio communications are both impacted by ionosphere changes caused by geomagnetic storms (Basu et al., 2001; Song et al., 2020; Fraley, 2020). Spacecraft exposed to energetic particles during solar energetic particle events and radiation belt enhancements could result in temporary operational irregularities, critical electronics failure, solar panels degradation, and optical systems like imagers and blinding of star trackers (<https://www.nasa.gov/>) (Baker et al., 2018; Ferguson et al., 2015). Thus, studying these extreme geomagnetic storms is essential not only to the scientific and technological importance but also to the global economy. The causes of such intense geomagnetic storms are understood as multiple ICME impacts in sequence or as merged regions (Koehn et al., 2022). The Carrington-type geomagnetic storms are generally associated with such scenarios (W. D. Gonzalez et al., 1999; B. Tsurutani et al., 2003; Hayakawa et al., 2022) (Tsurutani 2003, Hayakawa et al, 2022, Gonzalez et al., 1999)

Besides this, planar magnetic structures (PMSs) are frequently seen in CIRs and sheath regions caused by ICMEs. PMS refer to large-scale, sheet-like magnetic structures. Recently Shaikh et al. (2020) statistically examine the plasma properties within planar and non-planar ICME sheath regions. Moreover, Shaikh & Raghav (2022) studied planar and non-planar magnetic cloud (MC) regions. Their study found that planar sheaths and quasi-planar MC had enhanced IMF field strength, and greater average plasma temperature, density, thermal pressure, and magnetic pressure than non-planar sheaths and MCs. Their analysis demonstrates that strong compression is critical in the formation of PMS in sheath regions or MC regions. Their study also found that the strength of the southward/northward magnetic field component is almost twice as strong in the planar sheath and planar MC regions compared to respective non-planar regions. Therefore, it implies that planar ICME sheaths and MCs are expected to have enhanced geo-effectiveness compared to non-planar ICME substructures.

Kataoka et al. (2015) examined highly compressed ICME sheath region with strong southward magnetic fields both in the sheath and the ejecta, followed by a high-speed stream. They suggested that the highly compressed sheath region transformed into PMSs. Moreover, they proposed that the enhanced solar wind speed, magnetic field, and density

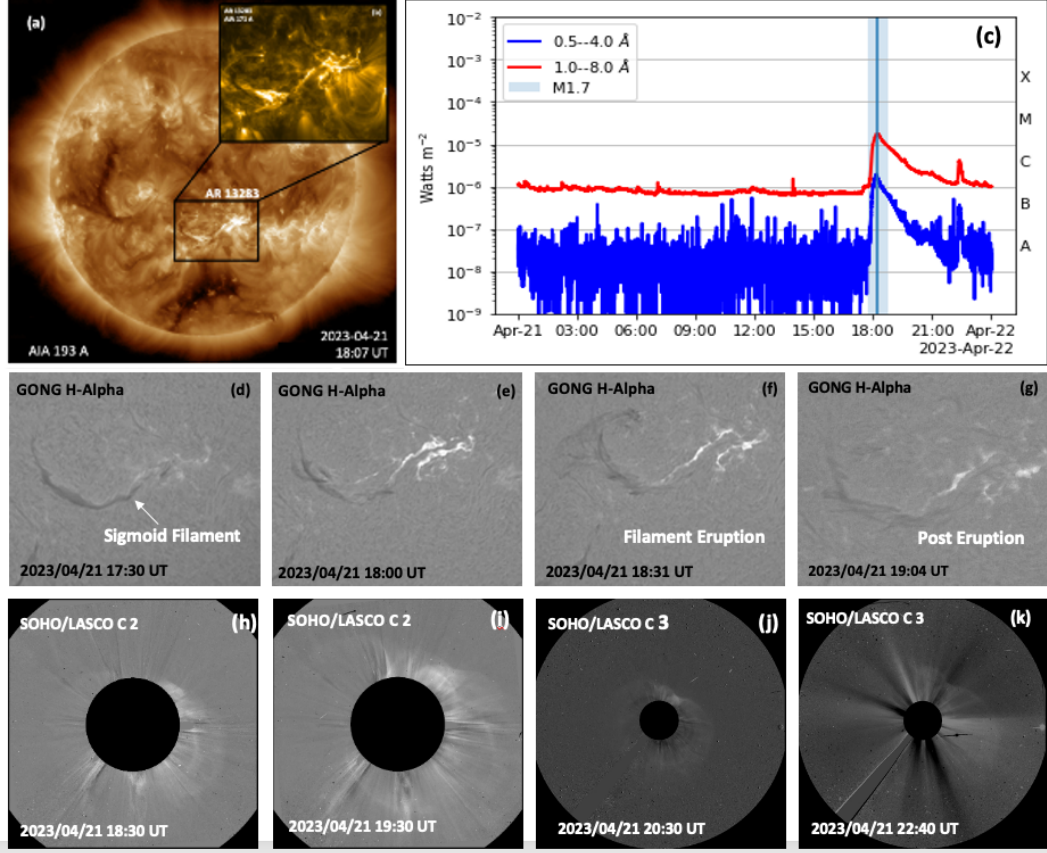


Figure 1. Top panel (a) SDO/AIA 171 Å filter image of source active region of CME-1 on 01 Nov 2021 18:38 UT, and zoom snap of AR 13283. (b) zoomed snap of the EUV AIA 304 Å images showing the flux rope eruption. (c) GOES X-ray plot for solar flare occurred on April 21, 2023, 17:44 UT. In the plot, the red curve shows the flux emission for energy bands 1-8 Å and the blue curve for 0.25-4 Å. Vertical line indicate the peak of flux (Class: M 1.7). Middle panel (d)-(g): GONG H-alpha observations, taken from Bi-Bear Observatory, CA, USA, present the sigmoid structure of filament, pre-eruption state, eruption and post eruption signatures respectively. Bottom panel, (h)-(i) Running-difference C2 images and (j)-(k) Running-difference C3 images showing the CME evolution up to 30 Rs

worked together to cause the major magnetic storm. Moreover, A. Raghav et al. (2023) examined the ICME properties that contributed to the super-storm of the century that occurred on 23 November 2003. The related ICME evolved like a quasi-PMSs referred to as pancaked ICME. They proposed that the presence of all observed increased characteristics with a large southbound magnetic field component helps to effectively transfer plasma and energy in the Earth’s magnetosphere, resulting in the reported superstorm.

On mid April 2023, the Solar Active region NOAA AR 13283, located at S20W15 at heliographic longitude was highly active and erupted a halo Coronal Mass Ejection (CME) on April 21, 2023 18:12 UT, which raced toward Earth and generate a intense geomagnetic storm at 19:26PM UT on April 23. We observe the source region activation and eruption of a filament by analyzing EUV, X-ray, $H\alpha$ and radio measurements. The SDO/AIA 193 Å observations (1 a) shows the emergence of a sigmoid filament structure with complex bundles of magnetic loops during the pre-eruption phase. The reported CME was associated with a

moderate flare which started at April 21, 17:44 UT and ends at 18:37 UT after reaching the peak with intensity class M1.7 at 18:12UT. This flare expels a billion tons of super-heated magnetized plasma into the interplanetary medium 1(c). In the lower corona, sigmoids result from drastically sheared magnetic structures that exhibit inverse-shaped patterns Rust & Kumar (1996). Numerous studies indicate these formations are extremely unstable and will eventually erupt (Canfield et al. (2007) and references within). This is followed by several episodes of coronal loop brightening and notable changes in the magnetic flux through the active region in different wavelength band observations. The filament that erupts with CME was present near the source active region for several hours before, during, and after the eruption of CME, and the active region presents a relatively stable form at after eruption. A twisted structure may erupt in all of AIA's coronal wavelengths around 18:30 UT. Various studies confirmed that one of the major factors that set off solar filament explosions is kink instability Török & Kliem (2003); Srivastava et al. (2010); Duchlev et al. (2018). However, the twist of the filament is difficult to measure, so we examine the high resolution $H\alpha$ images observed from Big-Bear GONG Observatory 1, (d)-(g), which clearly shows the pre and post-eruption signature on lower corona(1 b). A coronal hole also exists at the near active region at lower latitude; this may further impact the orientation of CME propagation into the interplanetary medium.

CME has a broad front and emerges swiftly at a plane of sky with the speed of 512 km s^{-1} in the LASCO/SOHO C2 observations. CME was low in the corona at roughly 18:30 UT on April 21, 2023 and it is 360° wide at the height of $6.2 R_s$ on 20:24 UT. As CME develops in the white-light coronagraphic field of view, in the LASCO C2 image, a similar structure can be seen the halo structure of CME (Figure 1 (h)-(i)). We identify this structure as a shock driven by CME. The evidence of the shock caused by CME can also be observed in sequence of coronagraphic images from SOHO/LASCO C3 (Figure 1 (j)-(k)). The driven shock becomes more visible as CME moves further outward in the corona.

In view of this event, we examine the cause of an extreme storm that occurred very recently, i.e., on 23 April 2023. The observed storm is found to be the first extreme storm of the 25th century which has several impacts on space weather. Many news reports claimed the Auroral activity at the low latitude region, e.g., Ladakh, India. We investigate the properties of ICME that lead to the storms.

Data and Method

To study the disturbed magnetospheric conditions, we have utilized the geomagnetic storm index, i.e., $Sym - H$ index. To analyze interplanetary structures that cause the disturbance in the magnetosphere, we have used data from OMNI database ¹. It provides interplanetary plasma and magnetic field data which is time-shifted data at Earth's bow-shock nose. The interplanetary magnetic field (IMF) ($B_T(nT)$), and their components B_x, B_y, B_z (nT) in GSM coordinate system. The plasma parameters includes, solar wind speed ($V_p(kms^{-1})$), and plasma temperature ($T(K)$), proton density ($N_p(cm^{-3})$), flow Pressure($P(nPa)$), and plasma beta (β). The $Sym - H$ index, plasma parameters, and magnetic field data have 1 *min* temporal resolution.

The PMS identification method has been discussed in detail by Nakagawa et al. (1989); Neugebauer et al. (1993); Palmerio et al. (2016); and references therein. Shaikh & Raghav (2022) used the same method and identified PMSs in ICME sheath and magnetic cloud. The region under examination must satisfy the following criteria in order to be a PMS: (1) wide distribution of the azimuth (ϕ) angle, i.e., $0^\circ < \phi < 360^\circ$, (2) good planarity, i.e., $|B_n|/B \leq 0.2$, and (3) good efficiency $R = \lambda_2/\lambda_3 \geq 3$ respectively (Palmerio et al., 2016);(Shaikh et al., 2019). Here, B is the magnitude of IMF, and B_n is the component of

¹ Available at <https://cdaweb.gsfc.nasa.gov/>

the magnetic field normal to the PMS plane i.e. $B_n = \vec{B} \cdot \hat{n}$, where \hat{n} is the normal direction of the PMS plane calculated by the MVA technique (Lepping & Behannon, 1980). The minimum variance analysis (MVA) technique has been employed to investigate the features of ICME and provides the direction along which the magnetic field variation is minimum. The MVA analysis gives three eigenvalues (λ_1, λ_2 , and λ_3) as output in descending order. Three eigenvectors (e_1, e_2 , and e_3) correspond to each eigenvalue, respectively. IMF vectors B_1^*, B_2^* , and B_3^* have been estimated after MVA analysis corresponding to the maximum, intermediate, and minimum variance direction. A PMS will have perfect planarity when $B_n = 0$. A low value of $|B_n|/B$ indicates that vectors are almost parallel to a plane (Neugebauer et al., 1993; Nakagawa et al., 1989).

1 Observations

1.1 Observations at L1

Figure 2 shows the temporal evolution of interplanetary plasma parameters and magnetic field from OMNI database. We observed the shock front on 23 April, 17.00. The ICME shock-front is recognized with sudden sharp enhancement in IMF (B_{mag}), solar wind speed (V_p), and proton density (N_p) (see the first vertical black dash line). The ICME sheath region is identified with high N_p , T_p , V_p , and plasma beta (β); large fluctuations in IMF vectors (i.e. $B_{x,y,z}$) (Kilpua et al., 2017; A. Raghav et al., 2014; A. N. Raghav & Kule, 2018b). The sheath lasts for 8 hours. The sheath is followed by lower fluctuations in B_{mag} and B_{comp} , slow rotation in θ and ϕ , the gradual decrease in V_p , indicating the transit of magnetic cloud of the ICME (Zurbuchen & Richardson, 2006; A. N. Raghav & Kule, 2018a,c; A. N. Raghav et al., 2018). The magnetic cloud onset is observed on 24 April, 01.00, and lasts for ~ 24 hours. The solar wind speed is nearly constant throughout the MC crossover, suggesting the negligible expansion of MC. The red and cyan shades depict the sheath and MC regions, respectively. Figure 3 represents hodogram plots in different projection planes after MVA transformation. The 2D hodogram represents a semicircular shape in the projection of intermediate and maximum planes. It clearly demonstrates the traditional magnetic cloud feature and suggests the smooth rotation of the magnetic field vector that represents the inbuilt feature of a magnetic cloud. We observed two steps extreme geomagnetic storm during the passage of ICME. The first step decrease of $\sim -175nT$ is visible in the sheath crossover. At magnetic cloud onset, we observe southward B_z , which results in the second step ($-231nT$) of the geomagnetic storm. We compare the observed Sym-H index with model estimates using Temerin & Li (2002) model, which is explicitly based on solar wind parameters. This empirical model reproduces an overall two-step profile of the observed geomagnetic storm. The model estimation is depicted in the bottom plot figure 2. However, the magnitude is overestimated.

1.2 PMS analysis

Figure 4 shows the $\theta-\phi$ distribution diagram for the complete ICME crossover region i.e. including shock-sheath and magnetic cloud. The fitted curve in $\theta-\phi$ is a typical signature of the possible existence of PMS. The estimated planarity ($|B_n|/B$) is 0.60 and the efficiency λ_2/λ_3 is 4.53. Note that, the shock sheath data points and MC data points follow the model curve depicted in Figure 4. Moreover, the scattered points of the trailing part of the magnetic cloud slowly deviate from the fitted model curve. Estimation suggest the planarity ($0.60 > 0.2$) is weak, but the fitted curve in the $\theta-\phi$ plot and efficiency ($3.85 > 3$) support the evolution of planar-like ICME; we refer to it as quasi-planar ICME. A high value of $|B_n|/B$ indicates that vectors are weakly parallel or quasi-parallel to a particular plane. Whereas in PMSs, the magnetic field vectors are almost confined to a particular plane, and that plane can rotate in any direction. The plane of observed quasi planar ICME inclined with respect to the ecliptic plane $\theta_{max} = 74.19^\circ$ and the normal direction of the plane is $\vec{n} = (-0.96, 0.25, 0.1)$. Figure 5 shows the results of PMS analysis for only the sheath region.

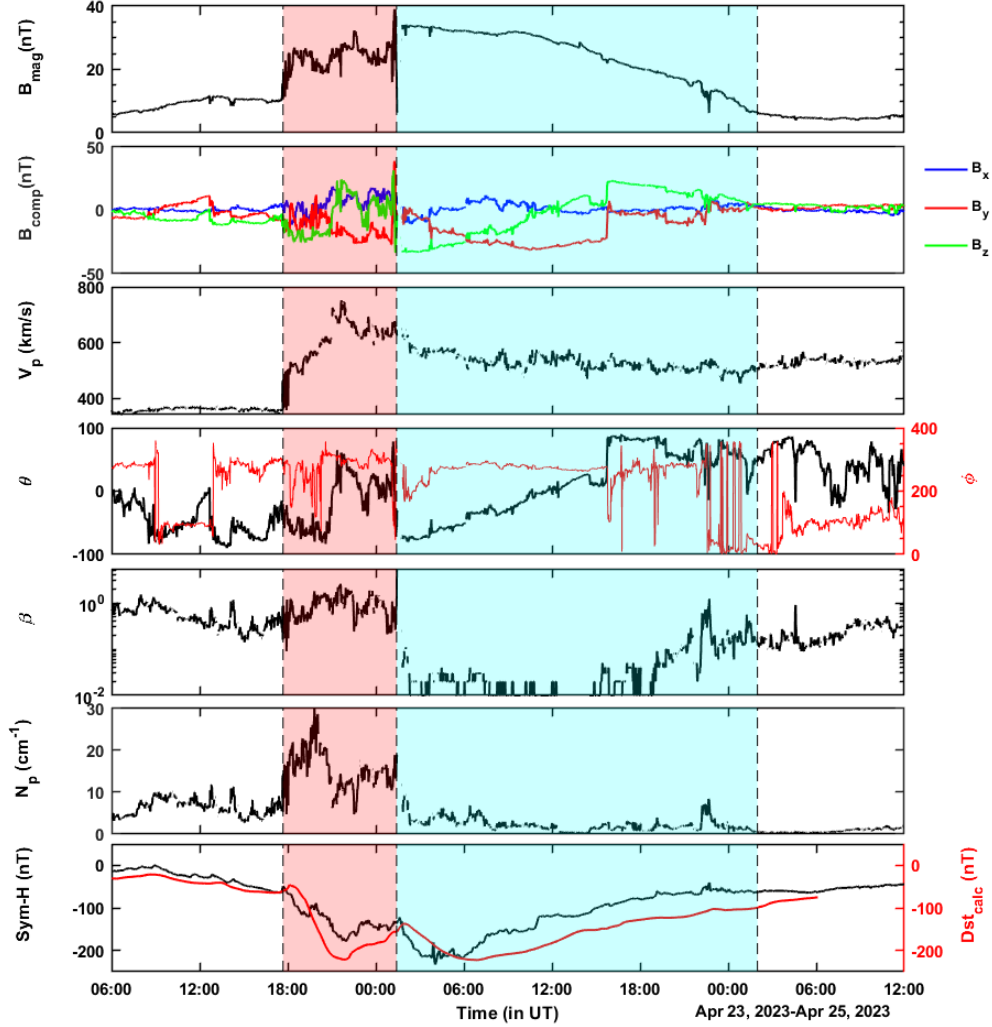


Figure 2. Top six panels show interplanetary parameters during ICME passage from 23-24 April 2023. The topmost panel display total interplanetary field strength (B_{mag}). The 2nd panel from the top shows variation in magnetic field components(B_x , B_y , B_z). The third panel demonstrate the speed of solar wind (V_p). The Fourth panel indicates the elevation angle (θ) and azimuth angle (ϕ) of the magnetic field vector. The fifth panel shows variation in plasma beta(β). The sixth panel shows the variation in proton number density (N_p) and the bottom panel shows the variation in geomagnetic storm index, i.e., $Sym - H$. The black line shows the observed $Sym - H$ index, and the red line shows model estimation by Temerin & Li (2002). The red-shaded region indicates the shock sheath and the cyan-shaded region indicates ICME magnetic cloud.

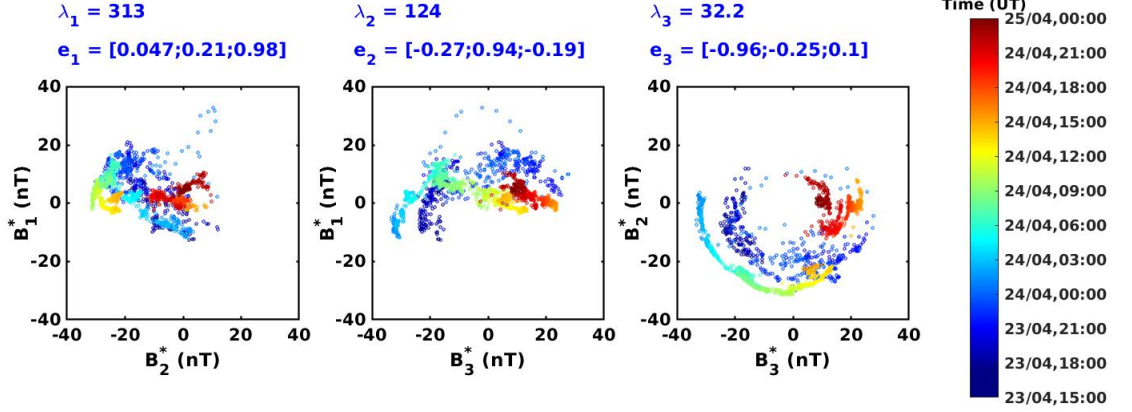


Figure 3. Hodogram plot of the ICME magnetic cloud region in a different plane of projections. B_{1*} , B_{2*} , and B_{3*} (corresponding to maximum (λ_1), intermediate (λ_2), and minimum (λ_3) eigenvalues) are the magnetic field vectors after MVA analysis

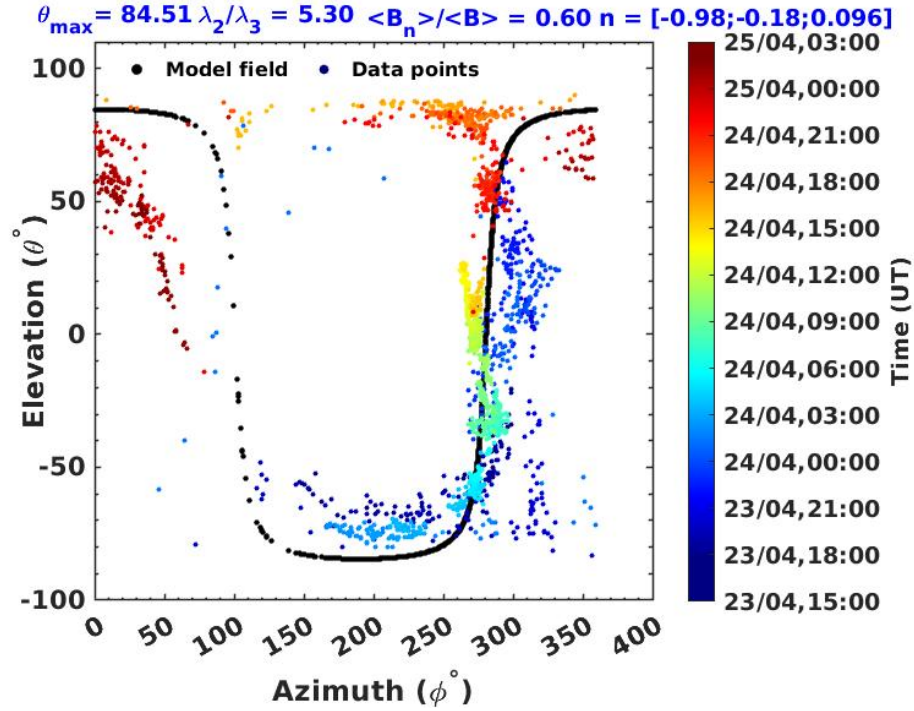


Figure 4. Distribution of azimuth (ϕ) vs elevation (θ) angle of IMF in GSM coordinate system for ICME magnetic cloud region (as shown in Figure 2). The λ_2/λ_3 , $\langle B_n \rangle / \langle B \rangle$, and n give the information about the efficiency, planarity, and normal direction of the PMS respectively. The θ_{max} is the inclination of the PMS plane w.r.t. the ecliptic plane. When IMF vectors $\vec{B} = (B_x, B_y, B_z) \equiv (B \cos \theta \cos \phi, B \cos \theta \sin \phi, B \sin \theta)$ are parallel to a plane whose normal is $\vec{n} \equiv (n_x, n_y, n_z)$, the relation between ϕ and θ is given as (Nakagawa et al., 1989; Palmerio et al., 2016): $n_x \cos \theta \cos \phi + n_y \cos \theta \sin \phi + n_z \sin \theta = 0$. The fitted curve (see the black dotted curve) to the measured (dotted coloured plot) ϕ and θ indicates the presence of PMS.

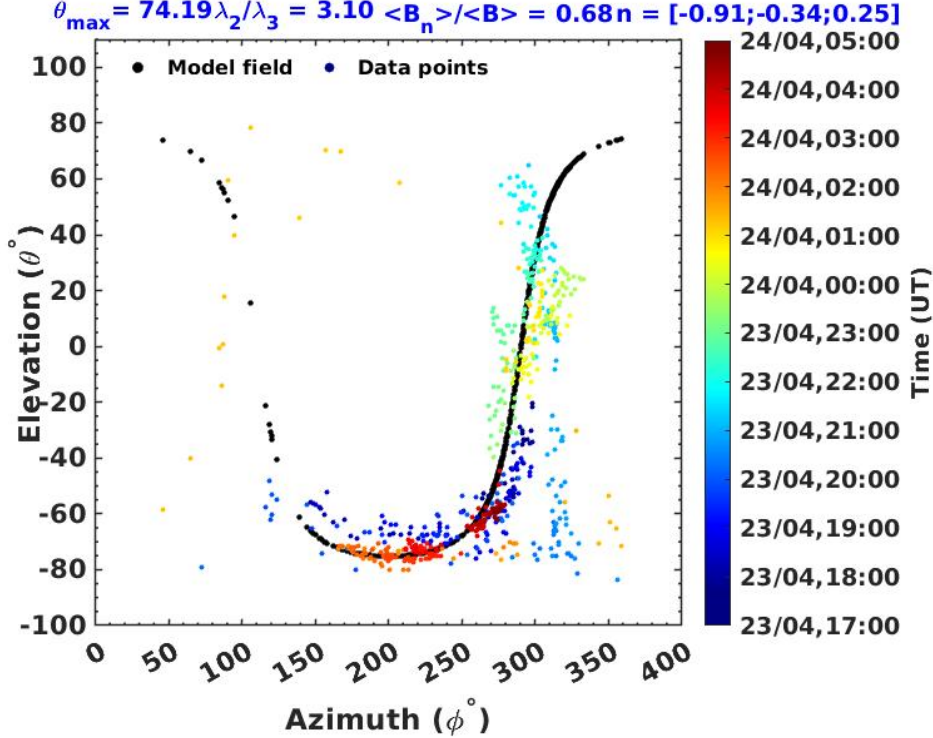


Figure 5. Distribution of azimuth (ϕ) vs elevation (θ) angle of IMF in GSM coordinate system for ICME sheath.

The estimated planarity ($|B_n| / \langle B \rangle$) is 0.68, and the efficiency λ_2/λ_3 is 3.10. Here also, we found the weak planarity in the sheath, but the fitted curve of $\theta - \phi$ and efficiency suggests the possible quasi-planar behaviour of the sheath.

Discussion and conclusion

Here, we observe that the PMS-like structure evolved within the ICME that crosses the earth on 23-24 April 2023. We observe the clear signature of the shock at the leading edge of ICME. However, the increase in proton number density, proton velocity, and plasma beta shows sheath is very compressed. A plasma pile-up might occur downstream of the shock, i.e. in the sheath. The planarity analysis for the sheath shows that the sheath transforms the quasi-planar structure. The pile-up of magnetic field and plasma in front of the magnetic cloud and the quasi-planar sheath might be responsible for the slow adiabatic expansion of the ICME. The average solar wind speed at the leading edge of MC (V_{LE}) is $\sim 610 \text{ km/s}^{-1}$. However, the solar wind speed at the trailing edge (V_{TE}) decreases to $\sim 510 \text{ km/s}^{-1}$. We observe that the difference between the solar wind speed at the leading and trailing edge of ICME is 100 km/s^{-1} . The expansion speed is calculated as (Owens et al., 2005):

$$V_{EXP} = \frac{V_{LE} - V_{TE}}{2}$$

The expansion speed is found to be $\sim 50 \text{ km/s}^{-1}$. This is minimal amongst the ICME's of $\sim 600 \text{ km/s}^{-1}$ speed (Owens et al., 2005). Moreover, we observe that the drop in solar wind velocity is between 23 April 2023, 1:25 UT, to 23 April 2023, 9:14 UT. This is the one-third region of the ICME magnetic cloud. The expansion speed for this region is observed to be $\sim 50 \text{ km/s}^{-1}$. The remaining two third region of the ICME magnetic cloud shows a flat solar wind speed profile of $\sim 500 \text{ km/s}^{-1}$. Therefore, the expansion speed was almost zero

for the next two-thirds region. This indicates that the ICME’s adiabatic expansion is nearly zero for the two-thirds region of the ICME magnetic cloud. This is observed to be unusual in the case of ICME, where the expansion speed at the trailing edge is higher in usual cases. We also observe the θ vs ϕ distribution for the total ICME follows the planarity curve (see Figure 4). Previously reported studies observed that the magnetic field variation of the flux rope observed from stationary spacecraft appears in the plane (Bothmer & Schwenn, 1997; Burlaga et al., 1981; Lepping & Behannon, 1980). Here, our observations suggest similar behavior in the observed magnetic cloud.

The primary cause of geomagnetic storms is associated with interplanetary structures with intense, long-duration, and southward magnetic fields (B_z). The coupling mechanism is the magnetic reconnection between southwardly directed IMF (B_z) and northward directed field at the magnetopause, which allows energy transport into the earth’s magnetosphere (W. D. Gonzalez et al., 1999; Dungey, 1961; W. Gonzalez & Mozer, 1974b). The strength of a geomagnetic storm depends on the strength of B_z . Moreover, the duration of the main phase of the geomagnetic storm is also related to how to prolong the B_z remains negative (Tang et al., 1989). In studied ICME event, we observe $B_{mag} \sim 25nT$, $B_z \sim -22nT$ in sheath region, whereas $B_{mag} \sim 35nT$, $B_z \sim -30nT$ in magnetic cloud region. The plasma pile-up in the compressed sheath region and weaker adiabatic expansion of the magnetic cloud could be the possible reason for the observed higher strength of the magnetic field. Shaikh et al. (2020) showed the magnitude of the total magnetic field (B_{mag}) of planar sheath events are higher than those of non-planar sheath events. Moreover, the strength of the southward component of IMF (B_z) for planar sheath events is almost double compared to non-planar sheath events. They suggest that the high compression of the sheath may cause the strengthening of the IMF within the planar sheath. This should be the main reason behind the intense geomagnetic storm that was observed due to PMS transforming ICME sheath.

The general profile of geomagnetic storms includes SSC, the main phase and the recovery phase. It is well known that the SSC was observed due to an enhancement in magneto-pause current. The northward component of the magnetic field interacts with the magnetosphere, which causes compression and increases the resultant magnetic field. In the studied case, the Sym-H index shows the absence of SSC. We observed the shifting of B_z southward during shock onset for nearly three hours, later, the B_z was found to be fluctuating during sheath crossover. This might be the cause of the first step of the extreme geomagnetic storm. This also might be the reason for the absence of SSC in this event. The presence of SSC is essential in space weather prediction due to its precursors observed in cosmic ray flux (Munakata et al., 2000). However, the absence of an SSC similar to a studied event may cause ambiguity in the domain of space weather predictions.

During magnetic cloud onset, the B_z again oriented southward. This could be the cause of the second step in the observed geomagnetic storm. The fluctuations in the orientation of B_z lead to the multistep in the main phase of the geomagnetic storm. Generally, the multistep main phase is observed in the successive crossing of the magnetic cloud, but sometimes it is observed during a single ICME crossover (I. Richardson & Zhang, 2008; Kamide, Yokoyama, et al., 1998). During multistep storms, the magnetosphere senses repeated disturbance in partially recovered conditions. This leads to the reactivation of the ring current soon after it started to recover from the passage of the first disturbance. This might be the reason for most intense and extreme geomagnetic storms. Due to the successive reconnections at the magnetopause, there might be changes in the magnetopause boundary. The quantitative estimates of these changes could be represented by empirical magnetopause models such as Shue et al. (1998). Figure 6 (b) shows the standoff magnetopause distance estimated using the empirical model by Shue et al. (1998) using OMNI data. The time series shows the magnetopause moved as close to as $\sim 6 Re$. Figure 6 shows the observational evidence of magnetopause crossing within the geosynchronous orbit. Figure 6 (a) indicates the orbital plot of GOES 16 and 17 satellites on 23 April 2023 18.00 UT.

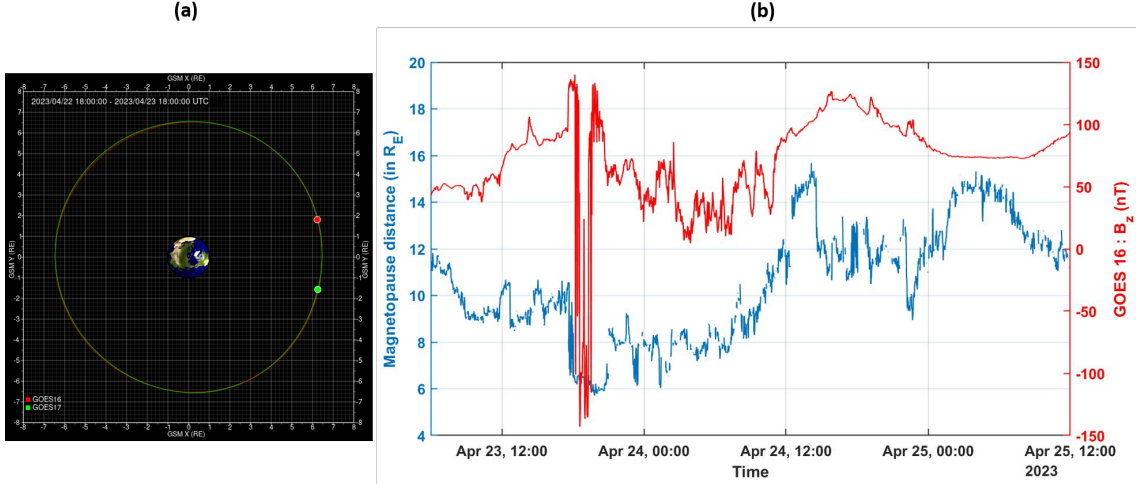


Figure 6. Left figure (a) shows the orbital plot of GOES 16 and 17 satellites on 23 April 2023 at 18.00 UT. The right figure (b) The temporal variation of estimated standoff magnetopause distance using Shue et al. (1998) and the B_z component of the magnetic field measured by GOES 16

Both the spacecraft were located on the dayside. We found that GOES 16 is almost near the nose of the magnetosphere. Figure 6 (b) depicts the B_z component of the magnetic field measured by GOES 16 (the data from GOES 17 is unavailable at this time). We found clear evidence of strong magnetic disturbance at 18.00 UT. The B_z polarity reversed for an hour. This is a clear observation showing MP crossed the geosynchronous orbit. This implies mostly all geosynchronous spacecraft in the day-side magnetosphere were exposed to the harsh interplanetary space environment.

Using Wind spacecraft data, A. N. Raghav & Shaikh (2020) provided the first confirmation of PMS molded ICME. They assumed that the higher aspect ratios are possible for ICMEs at 1 AU and demonstrated their effect on the cross-section, suggesting that a passage of a spacecraft through a highly flattened cross-section of the flux rope may be interpreted as a quasi-2D planar magnetic structure. However, it is also implied that the rotation of the magnetic field vector remains the intact feature of MC, and one should observe a semi-elliptical shape in the hodogram plot. Here, we suggest that the ICME to PMS transformation process leads to a weak adiabatic expansion of the magnetic cloud than expected, keeping a strong magnetic field within the magnetic cloud (in particular enhanced B_z component of IMF). This leads to the intensification of the parameters responsible for geomagnetic storms.

In conclusion, we investigate the first two-step extreme geomagnetic storms of the 25th solar cycle on April 23, 2023, with a Sym-H index of $-231nT$. We conclude that the ICME sheath transformed to the quasi-planar structure. We also observed weaker adiabatic expansion of the magnetic cloud than anticipated, maintaining the magnetic cloud's high speed, strong magnetic field (significantly enhanced B_z component) IMF, high dynamic pressure. The time series variation of standoff magnetopause distance estimated using the empirical model by Shue et al. (1998) shows the magnetosphere was highly compressed during the storm. The magnetopause boundary moved $< 6Re$, implies the deformation of the plasmasphere and radiation belt. The enhanced magnetic pressure inside the quasi-planar moulded ICME sheath could be the possible cause behind the observed significant erosion of the magnetosphere. The statistical investigation of the geo-effectiveness of these planar structures is necessary to support the reported outcome.

Acknowledgement

The utilised data in this analysis is taken from OMNI database. The data are publicly available at Coordinated Data Analysis Web (CDAWeb) <https://cdaweb.gsfc.nasa.gov/pub/data/wind/>. We acknowledge use of the NASA/GSFC for data availability. We also thank SOHO team for making data available in the public domain. KG is supported by the DST-INSPIRE fellowship [IF210212], and OD is supported by the SERB project (CRG/2020/002314).

References

- Akasofu, S.-I. (2018). A review of the current understanding in the study of geomagnetic storms. *International Journal of Earth Science and Geophysics*, *4*(1).
- Akasofu, S.-I., Chapman, S., & Venkatesan, D. (1963). The main phase of great magnetic storms. *Journal of Geophysical Research*, *68*(11), 3345–3350.
- Baker, D., Erickson, P., Fennell, J., Foster, J., Jaynes, A., & Verronen, P. (2018). Space weather effects in the earth’s radiation belts. *Space Science Reviews*, *214*(1), 1–60.
- Basu, S., Basu, S., Valladares, C., Yeh, H.-C., Su, S.-Y., MacKenzie, E., . . . others (2001). Ionospheric effects of major magnetic storms during the international space weather period of september and october 1999: Gps observations, vhf/uhf scintillations, and in situ density structures at middle and equatorial latitudes. *Journal of Geophysical Research: Space Physics*, *106*(A12), 30389–30413.
- Boerner, W.-M., Cole, J. B., Goddard, W. R., Tarnawecy, M. Z., Shafai, L., & Hall, D. H. (1983). Impacts of solar and auroral storms on power line systems. *Space Science Reviews*, *35*(2), 195–205.
- Boteler, D. (2003). Geomagnetic hazards to conducting networks. *Natural Hazards*, *28*(2), 537–561.
- Bothmer, V., & Schwenn, R. (1997). The structure and origin of magnetic clouds in the solar wind. In *Annales geophysicae* (Vol. 16, pp. 1–24).
- Burlaga, L. (1988). Magnetic clouds and force-free fields with constant alpha. *Journal of Geophysical Research: Space Physics*, *93*(A7), 7217–7224.
- Burlaga, L., Sittler, E., Mariani, F., & Schwenn, a. R. (1981). Magnetic loop behind an interplanetary shock: Voyager, helios, and imp 8 observations. *Journal of Geophysical Research: Space Physics*, *86*(A8), 6673–6684.
- Canfield, R. C., Kazachenko, M. D., Acton, L. W., Mackay, D., Son, J., & Freeman, T. L. (2007). Yohkoh sxt full-resolution observations of sigmoids: structure, formation, and eruption. *The Astrophysical Journal*, *671*(1), L81.
- Chapman, S., & Bartels, J. (1940). *Geomagnetism* (Vol. 2). Clarendon Press.
- Chapman, S., & Ferraro, V. (1931). Theory of magnetic storms. *Terr. Mag*, *36*(77-97), 171–186.
- Chapman, S., & VCA, F. (1931). A new theory of magnetic storms (sections 1–5). *Terr Magn Atmos Electr*, *36*(2), 77–97.
- Chen, M. W., Schulz, M., & Lyons, L. R. (1997). Modeling of ring current formation and decay: A review. *Washington DC American Geophysical Union Geophysical Monograph Series*, *98*, 173–186.
- Choraghe, K., Raghav, A., Chakrabarty, D., Kasthurirangan, S., & Bijewar, N. (2021). Properties of the recovery phase of extreme storms. *Journal of Geophysical Research: Space Physics*, *126*(9), e2020JA028685.
- Daglis, I. A., Thorne, R. M., Baumjohann, W., & Orsini, S. (1999). The terrestrial ring current: Origin, formation, and decay. *Reviews of Geophysics*, *37*(4), 407–438.
- Dessler, A., Francis, W., & Parker, E. (1960). Geomagnetic storm sudden-commencement rise times. *Journal of Geophysical Research*, *65*(9), 2715–2719.
- Duchlev, P., Dechev, M., & Koleva, K. (2018). Two different cases of filament eruptions driven by kink instability. *New Astronomy*, *59*, 45–53.

- Dungey, J. W. (1961). Interplanetary magnetic field and the auroral zones. *Physical Review Letters*, 6(2), 47.
- Echer, E., Gonzalez, W., Tsurutani, B., & Gonzalez, A. (2008). Interplanetary conditions causing intense geomagnetic storms ($\text{dst} \leq -100$ nt) during solar cycle 23 (1996–2006). *Journal of Geophysical Research: Space Physics*, 113(A5).
- Fairfield, D. H., & Cahill Jr, L. J. (1966). Transition region magnetic field and polar magnetic disturbances. *Journal of Geophysical Research*, 71(1), 155–169.
- Ferguson, D. C., Worden, S. P., & Hastings, D. E. (2015). The space weather threat to situational awareness, communications, and positioning systems. *IEEE Transactions on Plasma Science*, 43(9), 3086–3098.
- Fraley, E. (2020). *Us security threatened by solar storm impacts on earth-and space-based technologies*. CAI Student Research Reports. <https://www.usu.edu/cai/student-research>
- Frank, L. A. (1967). On the extraterrestrial ring current during geomagnetic storms. *Journal of Geophysical Research*, 72(15), 3753–3767.
- Gonzalez, W., Joselyn, J., Kamide, Y., Kroehl, H., Rostoker, G., Tsurutani, B., & Vasyliunas, V. (1994). What is a geomagnetic storm? *Journal of Geophysical Research: Space Physics*, 99(A4), 5771–5792.
- Gonzalez, W., & Mozer, F. (1974a). A quantitative model for the potential resulting from reconnection with an arbitrary interplanetary magnetic field. *Journal of Geophysical Research*, 79(28), 4186–4194.
- Gonzalez, W., & Mozer, F. (1974b). A quantitative model for the potential resulting from reconnection with an arbitrary interplanetary magnetic field. *Journal of Geophysical Research*, 79(28), 4186–4194.
- Gonzalez, W. D., Tsurutani, B. T., & De Gonzalez, A. L. C. (1999). Interplanetary origin of geomagnetic storms. *Space Science Reviews*, 88(3-4), 529–562.
- Hayakawa, H., Nevanlinna, H., Blake, S. P., Ebihara, Y., Bhaskar, A. T., & Miyoshi, Y. (2022). Temporal variations of the three geomagnetic field components at colaba observatory around the carrington storm in 1859. *The Astrophysical Journal*, 928(1), 32.
- Huttunen, K., Koskinen, H., Karinen, A., & Mursula, K. (2006). Asymmetric development of magnetospheric storms during magnetic clouds and sheath regions. *Geophysical research letters*, 33(6).
- Jordanova, V. K. (2020). Ring current decay. In *Ring current investigations* (pp. 181–223). Elsevier.
- Kamide, Y., Baumjohann, W., Daglis, I., Gonzalez, W., Grande, M., Joselyn, J., . . . others (1998). Current understanding of magnetic storms: Storm-substorm relationships. *Journal of Geophysical Research: Space Physics*, 103(A8), 17705–17728.
- Kamide, Y., McPherron, R., Gonzalez, W., Hamilton, D., Hudson, H., Joselyn, J., . . . Szuszczewicz, E. (1997). Magnetic storms: Current understanding and outstanding questions. *Magnetic storms*, 1–19.
- Kamide, Y., Yokoyama, N., Gonzalez, W., Tsurutani, B., Daglis, I., Brekke, A., & Masuda, S. (1998). Two-step development of geomagnetic storms. *Journal of Geophysical Research: Space Physics*, 103(A4), 6917–6921.
- Kataoka, R., Shiota, D., Kilpua, E., & Keika, K. (2015). Pileup accident hypothesis of magnetic storm on 17 march 2015. *Geophysical Research Letters*, 42(13), 5155–5161.
- Kilpua, E., Jian, L., Li, Y., Luhmann, J., & Russell, C. (2012). Observations of icmes and icme-like solar wind structures from 2007–2010 using near-earth and stereo observations. *Solar Physics*, 281(1), 391–409.
- Kilpua, E., Koskinen, H. E., & Pulkkinen, T. I. (2017). Coronal mass ejections and their sheath regions in interplanetary space. *Living Reviews in Solar Physics*, 14(1), 1–83.
- Koehn, G. J., Desai, R. T., Davies, E. E., Forsyth, R. J., Eastwood, J. P., & Poedts, S. (2022). Successive interacting coronal mass ejections: How to create a perfect storm. *The Astrophysical Journal*, 941(2), 139.
- Koskinen, H., & Huttunen, K. (2006). Geoeffectivity of coronal mass ejections. *Space*

- science reviews*, 124(1), 169–181.
- Kozyra, J. U., & Liemohn, M. W. (2003). Ring current energy input and decay. *Magnetospheric Imaging—the Image Prime Mission*, 105–131.
- Krieger, A., Timothy, A., & Roelof, E. (1973). A coronal hole and its identification as the source of a high velocity solar wind stream. *Solar Physics*, 29(2), 505–525.
- Lepping, R., & Behannon, K. (1980). Magnetic field directional discontinuities: 1. minimum variance errors. *Journal of Geophysical Research: Space Physics*, 85(A9), 4695–4703.
- Marusek, J. A. (2007). *Solar storm threat analysis*. J. Marusek.
- Munakata, K., Bieber, J. W., Yasue, S.-i., Kato, C., Koyama, M., Akahane, S., . . . Duldig, M. L. (2000). Precursors of geomagnetic storms observed by the muon detector network. *Journal of Geophysical Research: Space Physics*, 105(A12), 27457–27468.
- Nakagawa, T., Nishida, A., & Saito, T. (1989). Planar magnetic structures in the solar wind. *Journal of Geophysical Research: Space Physics*, 94(A9), 11761–11775.
- Neugebauer, M., Clay, D., & Gosling, J. (1993). The origins of planar magnetic structures in the solar wind. *Journal of Geophysical Research: Space Physics*, 98(A6), 9383–9389.
- O’Brien, T. P., & McPherron, R. L. (2000). An empirical phase space analysis of ring current dynamics: Solar wind control of injection and decay. *Journal of Geophysical Research: Space Physics*, 105(A4), 7707–7719.
- Owens, M. J., Cargill, P., Pagel, C., Siscoe, G., & Crooker, N. (2005). Characteristic magnetic field and speed properties of interplanetary coronal mass ejections and their sheath regions. *Journal of Geophysical Research: Space Physics*, 110(A1).
- Palmerio, E., Kilpua, E. K., & Savani, N. P. (2016). Planar magnetic structures in coronal mass ejection-driven sheath regions. In *Annales geophysicae* (Vol. 34, pp. 313–322).
- Raghav, A., Bhaskar, A., Lotekar, A., Vichare, G., & Yadav, V. (2014). Quantitative understanding of forrush decrease drivers based on shock-only and cme-only models using global signature of february 14, 1978 event. *Journal of Cosmology and Astroparticle Physics*, 2014(10), 074.
- Raghav, A., Shaikh, Z., Vemareddy, P., Bhaskar, A., Dhamane, O., Ghag, K., . . . Mohammed Al Suti, B. (2023). The possible cause of most intense geomagnetic superstorm of the 21st century on 20 november 2003. *Solar Physics*, 298(5), 64.
- Raghav, A. N., Choraghe, K., & Shaikh, Z. I. (2019). The cause of an extended recovery from an icme-induced extreme geomagnetic storm: a case study. *Monthly Notices of the Royal Astronomical Society*, 488(1), 910–917.
- Raghav, A. N., & Kule, A. (2018a). Does the alfvén wave disrupt the large-scale magnetic cloud structure? *Monthly Notices of the Royal Astronomical Society: Letters*, 480(1), L6–L11.
- Raghav, A. N., & Kule, A. (2018b). The first in situ observation of torsional alfvén waves during the interaction of large-scale magnetic clouds. *Monthly Notices of the Royal Astronomical Society: Letters*, 476(1), L6–L9.
- Raghav, A. N., & Kule, A. (2018c). The first insitu observation of torsional alfvén waves during the interaction of large-scale magnetic clouds. *Monthly Notices of the Royal Astronomical Society: Letters*.
- Raghav, A. N., Kule, A., Bhaskar, A., Mishra, W., Vichare, G., & Surve, S. (2018). Torsional alfvén wave embedded icme magnetic cloud and corresponding geomagnetic storm. *The Astrophysical Journal*, 860(1), 26.
- Raghav, A. N., & Shaikh, Z. I. (2020). The pancaking of coronal mass ejections: an in situ attestation. *Monthly Notices of the Royal Astronomical Society: Letters*, 493(1), L16–L21.
- Richardson, I., Webb, D., Zhang, J., Berdichevsky, D., Biesecker, D., Kasper, J., . . . others (2006). Major geomagnetic storms (dst = - 100 nt) generated by corotating interaction regions. *Journal of Geophysical Research: Space Physics*, 111(A7).
- Richardson, I., & Zhang, J. (2008). Multiple-step geomagnetic storms and their interplanetary drivers. *Geophysical research letters*, 35(6).
- Richardson, I. G., & Cane, H. V. (2012). Solar wind drivers of geomagnetic storms during

- more than four solar cycles. *Journal of Space Weather and Space Climate*, 2, A01.
- Rust, D. M., & Kumar, A. (1996). Evidence for helically kinked magnetic flux ropes in solar eruptions. *The Astrophysical Journal*, 464(2), L199.
- Schwenn, R., Dal Lago, A., Huttunen, E., & Gonzalez, W. D. (2005). The association of coronal mass ejections with their effects near the earth. In *Annales geophysicae* (Vol. 23, pp. 1033–1059).
- Shaikh, Z. I., Raghav, A., & Vichare, G. (2019). Coexistence of a planar magnetic structure and an alfvén wave in the shock-sheath of an interplanetary coronal mass ejection. *Monthly Notices of the Royal Astronomical Society*, 490(2), 1638–1643.
- Shaikh, Z. I., & Raghav, A. N. (2022). Statistical plasma properties of the planar and nonplanar icme magnetic clouds during solar cycles 23 and 24. *The Astrophysical Journal*, 938(2), 146.
- Shaikh, Z. I., Raghav, A. N., Vichare, G., Bhaskar, A., & Mishra, W. (2020). Comparative statistical study of characteristics of plasma in planar and non-planar icme sheaths during solar cycles 23 and 24. *Monthly Notices of the Royal Astronomical Society*, 494(2), 2498–2508.
- Sheeley, N., Harvey, J., & Feldman, W. (1976). Coronal holes, solar wind streams, and recurrent geomagnetic disturbances: 1973–1976. *Solar Physics*, 49(2), 271–278.
- Shue, J.-H., Song, P., Russell, C., Steinberg, J., Chao, J., Zastenker, G., . . . others (1998). Magnetopause location under extreme solar wind conditions. *Journal of Geophysical Research: Space Physics*, 103(A8), 17691–17700.
- Smith, P., & Hoffman, R. A. (1973). Ring current particle distributions during the magnetic storms of december 16–18, 1971. *Journal of Geophysical Research*, 78(22), 4731–4737.
- Song, X., Yang, R., & Zhan, X. (2020). An analysis of global ionospheric disturbances and scintillations during the strong magnetic storm in september 2017. *Aerospace Systems*, 3(4), 255–263.
- Srivastava, A., Zaqarashvili, T., Kumar, P., & Khodachenko, M. (2010). Observation of kink instability during small b5. 0 solar flare on 2007 june 4. *The Astrophysical Journal*, 715(1), 292.
- Tang, F., Tsurutani, B. T., Gonzalez, W. D., Akasofu, S. I., & Smith, E. J. (1989). Solar sources of interplanetary southward bz events responsible for major magnetic storms (1978-1979). *Journal of Geophysical Research: Space Physics*, 94(A4), 3535–3541.
- Temerin, M., & Li, X. (2002). A new model for the prediction of dst on the basis of the solar wind. *Journal of Geophysical Research: Space Physics*, 107(A12), SMP–31.
- Török, T., & Kliem, B. (2003). The evolution of twisting coronal magnetic flux tubes. *Astronomy & Astrophysics*, 406(3), 1043–1059.
- Tsurutani, B., Gonzalez, W., Lakhina, G., & Alex, S. (2003). The extreme magnetic storm of 1–2 september 1859. *Journal of Geophysical Research: Space Physics*, 108(A7).
- Tsurutani, B., Lakhina, G., Verkhoglyadova, O. P., Gonzalez, W., Echer, E., & Guarnieri, F. (2011). A review of interplanetary discontinuities and their geomagnetic effects. *Journal of Atmospheric and Solar-Terrestrial Physics*, 73(1), 5–19.
- Tsurutani, B. T., Gonzalez, W. D., Gonzalez, A. L., Guarnieri, F. L., Gopalswamy, N., Grande, M., . . . others (2006). Corotating solar wind streams and recurrent geomagnetic activity: A review. *Journal of Geophysical Research: Space Physics*, 111(A7).
- Zurbuchen, T. H., & Richardson, I. G. (2006). In-situ solar wind and magnetic field signatures of interplanetary coronal mass ejections. *Coronal mass ejections*, 31–43.